

https://doi.org/10.1070/QEL17971

YAG:R^{3+} (R = Ce, Dy, Yb) nanophosphor-based luminescent fibre-optic sensors for temperature measurements in the range 20–500 °C

S.K. Evstropiev, V.V. Demidov, D.V. Bulyga, R.V. Sadovnichii, G.A. Pchelkin, D.N. Shurupov, Yu.F. Podrukhin, A.S. Matrosova, N.V. Nikonorov, K.V. Dukelskii

Abstract. **We report the development of a group of luminescent fibre-optic temperature sensors that use Ce^{3+}-, Dy^{3+}-, and Yb^{3+}-doped yttrium aluminium garnet (YAG) nanophosphors as thermosensitive materials. The nanophosphors have been prepared in the form of powders with a crystallite size from 19 to 27 nm by a polymer–salt method and exhibit bright luminescence at 550 (YAG:Ce^{3+}), 400, 480 (YAG:Dy^{3+}), and 1030 nm (YAG:Yb^{3+}). The sensor design includes a silica capillary, partially filled with a nanophosphor, and two large-aperture multimode optical fibres located in the capillary, which deliver excitation light and receive and transmit the photoluminescence signal. The photoluminescence signal amplitude of all the sensors decreases exponentially with increasing temperature, pointing to characteristic thermal quenching of photoluminescence and adequate operation of the devices up to 500 °C. The highest temperature sensitivity among the fibre-optic sensors is offered by the YAG:Ce^{3+} nanophosphor-based devices.**

S.K. Evstropiev Vavilov State Optical Institute, ul. Babushkina 36/1, 192171 St. Petersburg, Russia; Bauman Moscow State Technical University, Vtoraya Baumanskaya ul. 5/1, 105005 Moscow, Russia; St. Petersburg National Research University of Information Technologies, Mechanics and Optics, Kronverkskii prosp. 49A, 197101 St. Petersburg, Russia; St. Petersburg State Institute of Technology (Technical University), Moskovskii pr. 26, 190013 St. Petersburg, Russia;
V.V. Demidov, R.V. Sadovnichii Vavilov State Optical Institute, ul. Babushkina 36/1, 192171 St. Petersburg, Russia; Bauman Moscow State Technical University, Vtoraya Baumanskaya ul. 5/1, 105005 Moscow, Russia; e-mail: demidov@goi.ru;
D.V. Bulyga, N.V. Nikonorov St. Petersburg National Research University of Information Technologies, Mechanics and Optics, Kronverkskii prosp. 49A, 197101 St. Petersburg, Russia;
G.A. Pchelkin Vavilov State Optical Institute, ul. Babushkina 36/1, 192171 St. Petersburg, Russia; Bauman Moscow State Technical University, Vtoraya Baumanskaya ul. 5/1, 105005 Moscow, Russia; Bonch-Bruevich St. Petersburg State University of Telecommunications, prosp. Bol'shevikov 22/1, 193232 St. Petersburg, Russia;
D.N. Shurupov Vavilov State Optical Institute, ul. Babushkina 36/1, 192171 St. Petersburg, Russia; Peter the Great St. Petersburg Polytechnic University, Politekhnicheskaya ul. 29, 195251 St. Petersburg, Russia;
Yu.F. Podrukhin Peter the Great St. Petersburg Polytechnic University, Politekhnicheskaya ul. 29, 195251 St. Petersburg, Russia;
A.S. Matrosova Vavilov State Optical Institute, ul. Babushkina 36/1, 192171 St. Petersburg, Russia; Bauman Moscow State Technical University, Vtoraya Baumanskaya ul. 5/1, 105005 Moscow, Russia; St. Petersburg National Research University of Information Technologies, Mechanics and Optics, Kronverkskii prosp. 49A, 197101 St. Petersburg, Russia;
K.V. Dukelskii Vavilov State Optical Institute, ul. Babushkina 36/1, 192171 St. Petersburg, Russia; St. Petersburg National Research University of Information Technologies, Mechanics and Optics, Kronverkskii prosp. 49A, 197101 St. Petersburg, Russia; Bonch-Bruevich St. Petersburg State University of Telecommunications, prosp. Bol'shevikov 22/1, 193232 St. Petersburg, Russia

Received 28 October 2021; revision received 12 November 2021
Kvantovaya Elektronika **52** (1) 94–99 (2022)
Translated by O.M. Tsarev

Keywords: *fibre-optic sensor, temperature, capillary, multimode optical fibre, nanophosphor, yttrium aluminium garnet, cerium, dysprosium, ytterbium, photoluminescence, sensitivity.*

1. Introduction

High-temperature ($T > 400$ °C) temperature sensors have found wide application in industry and transport [1–4]. Temperature measurements with fibre-optic sensors (FOS's) have a number of advantages over measurements with other types of devices, primarily electrical ones. In particular, FOS's are compact, light, and electrically safe and ensure environment-parameter measurements localised at one point or distributed over the entire length of optical fibre [5]. The advantages of high-temperature FOS's include a broad range of working temperatures, good corrosion and vibration resistance, and insensitivity to strong electromagnetic fields [3].

To date, various types of high-temperature FOS's have been designed, which were the subject of reviews by Lin et al. [3] and Zhao et al. [6]. Usually, precision optical elements, e.g. Bragg gratings [1, 2] and Mach–Zehnder interferometers [6], are used as a thermosensitive material of such FOS's. Such optical elements are technologically and structurally complex, so they inherently carry an increased risk of being damaged during service under extreme conditions (high temperature, high/low temperature cycles, gaseous media with various chemical compositions, and other unfavourable factors). Thus, the necessity of monitoring high temperatures in various objects for industrial and civil applications, in combination with the long time needed for the measurement process and, often, the inaccessibility of the monitoring zone, requires the use of materials that have high thermal stability and are technologically attractive.

In recent years, considerable attention has been paid to the fabrication of luminescent FOS's converting shorter wavelength light in the UV, visible, or near-IR spectral region to longer wavelength light through photoluminescence. The key advantages of such devices are their short response time

and high sensitivity [7]. The operation of luminescent fibre optic (FO) temperature sensors is based on monitoring temperature-induced changes (quenching) of the photoluminescence of rare-earth ions in a thermosensitive material [8].

The purpose of this work was to produce and investigate a group of high-temperature luminescent FO temperature sensors having a simple design and insensitive to electromagnetic fields and gaseous environments. The main idea was to use YAG:R^{3+} (R = Ce, Dy, Yb) nanophosphors, offering bright photoluminescence in different spectral regions, and a large-aperture multimode fibre, receiving a photoluminescence signal, in a silica capillary. YAG was chosen as a matrix for nanophosphors because it has high thermal stability (up to 1940 °C) [9], is easy to dope with various rare-earth ions in order to obtain photoluminescence in the visible and near-IR spectral regions, and can luminesce in a wide temperature range, including relatively high temperatures (up to 800 °C) [10]. In addition, note that the possibility to synthesise efficient YAG:Ce^{3+} and YAG:Yb^{3+} nanophosphors was examined by us in Refs [11, 12]. The possibility of using YAG:Dy^{3+} as a luminescent thermosensitive material was pointed out in Refs [13, 14].

2. Synthesis and characterisation of the nanophosphors

YAG:R^{3+} (R = Ce, Dy, Yb) nanophosphor powders were prepared by a polymer–salt method [11, 12, 15]. The starting reagents used were aqueous solutions of high-purity (99.99%) yttrium, aluminium, cerium, and dysprosium nitrates [$Y(NO_3)_3$, $Al(NO_3)_3$, $Ce(NO_3)_3$, and $Dy(NO_3)_3$] and ytterbium sulphate [$Yb_2(SO_4)_3$]. An appropriate volume ratio of the solutions was mixed with an aqueous solution of high molecular weight polyvinylpyrrolidone (PVP10, average molecular weight of 10 000, Sigma Aldrich), which served, on the one hand, as a stabilising agent for YAG crystal formation, preventing uncontrolled crystal growth and aggregation, and, on the other, as additional fuel for the decomposition (combustion) of the metal salts during the synthesis process, thereby ensuring good luminescence properties of the material [16]. The chemical compositions of the starting solutions are given in Table 1.

After thorough stirring for 30 min and homogenisation, the starting solutions were dried in a drying oven at a temperature of 70 °C for 24 h and then heat-treated in a muffle furnace at 1000 °C for 2 h. These stirring, drying, and heat treatment conditions helped obtain homogeneous, highly dispersed YAG powders containing about 1 wt% R^{3+} (R = Ce, Dy, Yb) activator. Figure 1 shows scanning electron microscopy (SEM) images (Tescan Analytics VEGA3) of the synthesised YAG:Yb^{3+} and YAG:Ce^{3+} powders. It is seen that the powders consist of weakly aggregated particles 30–50 nm in size.

a

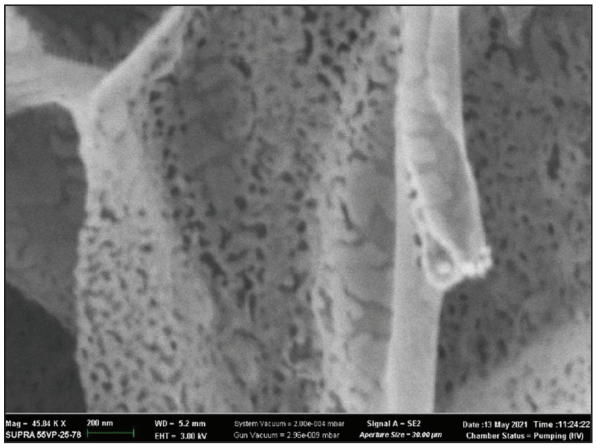

b

Figure 1. SEM images of the synthesised (a) YAG:Yb^{3+} and (b) YAG:Ce^{3+} nanophosphors.

Figure 2 shows X-ray diffraction (XRD) patterns of the nanophosphors (Rigaku Ultima IV high-resolution X-ray diffractometer). The data demonstrate two key features. First, the synthesised materials consist of only YAG crystals, which ensures the highest luminescence intensity at the activator concentration achieved. Second, the peak positions in the XRD patterns depend on the type of activator ion: In going from Yb to Dy and to Ce, the peaks shift slightly to smaller 2θ angles, because the ionic radii of the elements under consideration increase in going from Yb to Ce as a result of the YAG lattice expansion upon isomorphous substitution of Yb^{3+}, Dy^{3+}, or Ce^{3+} ions for Y^{3+} and the associated increase in interplanar spacings. For this reason, according to the Bragg–Wulff formula, the diffraction angle decreases.

Table 1. Chemical compositions of the starting solutions for the preparation of YAG:R^{3+} (R = Ce, Dy, Yb) nanophosphors.

Nanophosphor	Chemical composition of the starting solutions (wt %)						
	$Y(NO_3)_3$	$Al(NO_3)_3$	PVP10	Water	$Ce(NO_3)_3$	$Dy(NO_3)_3$	$Yb_2(SO_4)_3$
YAG:Ce^{3+}	1.56	2.01	4.49	91.92	0.02	–	–
YAG:Dy^{3+}	1.56	2.01	4.49	91.92	–	0.02	–
YAG:Yb^{3+}	1.56	2.01	4.49	91.92	–	–	0.02

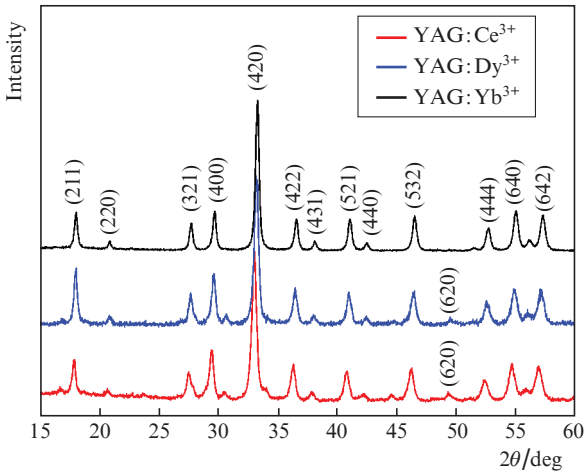

Figure 2. (Colour online) XRD patterns of the synthesised YAG:Ce^{3+}, YAG:Dy^{3+}, and YAG:Yb^{3+} nanophosphors.

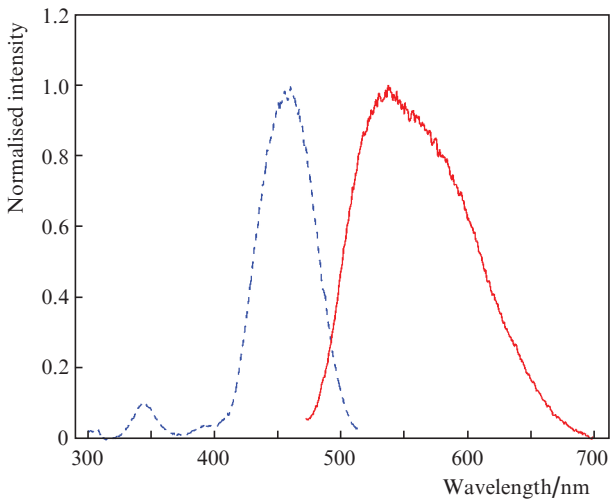

Figure 3. Excitation (dashed line) and luminescence (solid line) spectra of the YAG:Ce^{3+} nanophosphor.

Table 2 lists the unit-cell parameters and average crystallite sizes of the synthesised YAG:R^{3+} (R = Ce, Dy, Yb) nanophosphors. The average crystallite size was evaluated using the Scherrer equation [17]: $d = k\lambda/(\beta\cos\theta)$, where d is the sought crystallite size; k is a dimensionless particle shape factor ($k = 0.9$); λ is the X-ray wavelength (Cu Kα radiation, λ = 0.15406 nm); β is the full width at half maximum of the diffraction peak; and θ is the diffraction angle (Bragg angle). It is seen from Table 2 that the unit-cell parameters a and V of the nanophosphors exceed those of the pure (undoped) YAG single crystal. This points to lattice expansion upon substitution of Ce^{3+}, Dy^{3+}, and Yb^{3+} larger ions for Y^{3+}. The average crystallite size (19–27 nm) supports the conclusion drawn from the SEM results that there is insignificant particle aggregation.

Figures 3–5 show luminescence and excitation spectra of the synthesised nanophosphors. In particular, Fig. 3 shows excitation (peak position near 450 nm) and luminescence (peak position near 550 nm) spectra of the YAG:Ce^{3+} powder. The observed luminescence band corresponds to a $5d^1$–$4f^1$ electronic transition [11]. The photoluminescence spectra obtained for the YAG:Dy^{3+} powder at excitation wavelengths of 250 and 360 nm (Fig. 4) have bands peaking near 400 and 480 nm. The luminescence band peaking at 400 nm corresponds to the $^4I_{13/2}$–$^6H_{15/2}$ electronic transition, and the band peaking at 480 nm corresponds to the $^4F_{9/2}$–$^6H_{15/2}$ transition [20]. Figure 5 shows the excitation (peak positions at 940 and 975 nm) and luminescence (main peak at 1030 nm) spectra of the YAG:Yb^{3+} powder. Its photoluminescence spectrum contains additional bands with local maxima near 1010 and 1050 nm. The three bands are characteristic of ytterbium ions in a YAG matrix and correspond to the $^2F_{5/2}$–$^2F_{7/2}$ electronic transition [12].

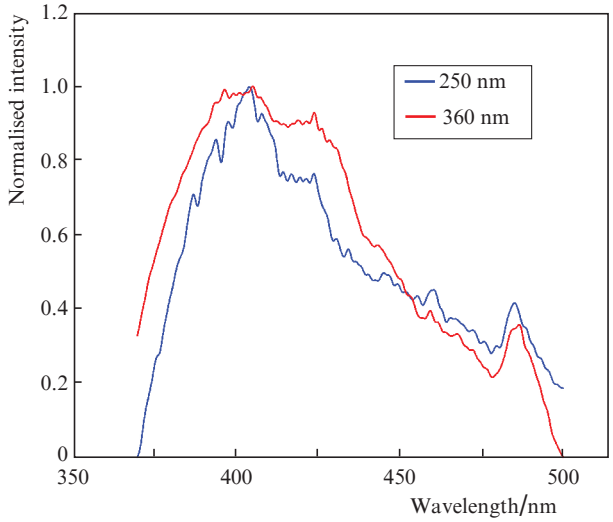

Figure 4. (Colour online) Photoluminescence spectra of the YAG:Dy^{3+} nanophosphor at excitation wavelengths of 250 and 360 nm.

The excitation and luminescence spectra of the YAG:Ce^{3+} and YAG:Dy^{3+} powders were measured in the range 250–800 nm using a PerkinElmer LS50B luminescence spectrometer. YAG:Yb^{3+} luminescence was excited by semiconductor laser pulses (pulse duration, 80 μs; wavelength λ = 975 nm) and detected using an Acton-300 monochromator (Acton Research) and ID-44 InGaAs photodetector (Acton Research). Prior to the measurements, the powders were tightly sandwiched between two plane-parallel polished silica

Table 2. Unit-cell parameters and average crystallite size of the synthesised YAG:R^{3+} (R = Ce, Dy, Yb) nanophosphors.

Material	Crystalline ionic radius of the dopant/Å [18]	$a = b = c$/Å	V/Å^3	Average crystallite size/nm
YAG:Ce^{3+} nanophosphor	1.28	12.0547(10)	1751.73(40)	19
YAG:Dy^{3+} nanophosphor	1.17	12.0495(16)	1749.47(68)	23
YAG:Yb^{3+} nanophosphor	1.12	12.0247(7)	1738.71(31)	27
YAG single crystal [19]	1.16 (Y)	12.002(2)	1728.86(9)	–

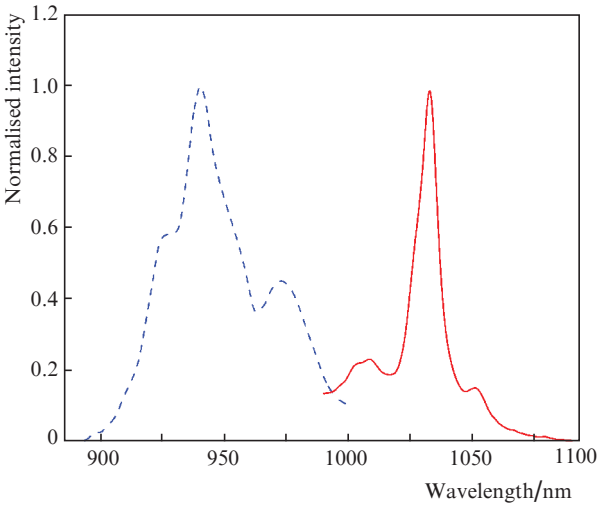

Figure 5. Excitation (dashed line) and luminescence (solid line) spectra of the YAG:Yb^{3+} nanophosphor.

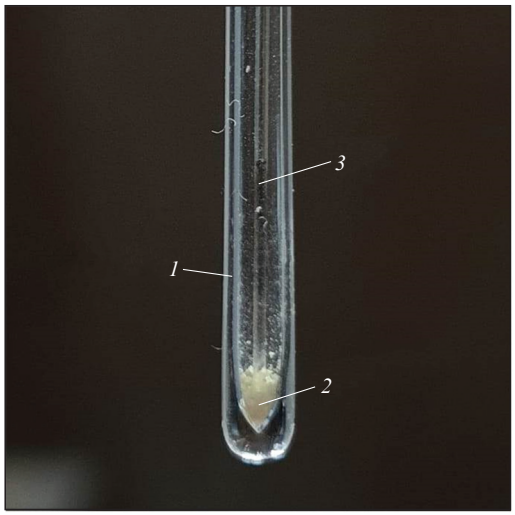

Figure 6. (Colour online) Photograph of the thermosensitive part of the luminescent FO temperature sensor:
(*1*) silica capillary; (*2*) nanophosphor; (*3*) large-aperture multimode optical fibre.

plates so that the thickness of the nanopowder layer was 150 μm.

The above materials characterisation results demonstrate that a group of YAG-based nanophosphors capable of operating in the visible and near-IR spectral regions have been prepared by the polymer–salt method. The feasibility of utilising them as thermosensitive materials of luminescent FOS's for temperature measurements can be assessed from results on the thermal quenching of photoluminescence for each activator in YAG.

3. Sensor design and characteristics

Initially, the luminescent FO temperature sensor included a 1.3-m-long multimode optical fibre having a 200-μm-diameter KUVI silica core with a numerical aperture of 0.22 and Sn protective coating. The fibre was placed in a 45-mm-long silica capillary with an inner diameter of 0.8 mm, fusion-sealed at one end (Fig. 6). The fusion-sealed end was filled with nanophosphor powder, which formed a 3-mm-thick layer, and a polished end face of the fibre, prestripped of its protective coating over a 20-mm-length, was brought close to the powder. The opposite end of the fibre was connected to receiving equipment.

Using an FOS having this design and containing the YAG:Ce^{3+} nanophosphor with a Ce^{3+} concentration of about 1 wt%, we studied the temperature dependence of the photoluminescence signal amplitude (in effect, the temperature sensitivity of the FOS). To this end, we used an experimental setup schematised in Fig. 7. Heat was delivered to the nanophosphor-filled part of the capillary by heating 1-mm-diameter Kh20N80 Nichrome wire wound in the form of two coils onto the capillary. The heating of the wire was controlled by applying a voltage from a laboratory autotransformer. Excitation light from a mercury lamp whose spectrum contained the luminescence excitation wavelength of the YAG:Ce^{3+} powder (λ = 450 nm) was directed (with no focusing lens) to the capillary. The 550-nm photoluminescence signal amplitude was measured as a function of temperature by a silicon photodiode operating in the spectral range 400–900 nm. Next, the signal was fed to an optical amplifier and digital oscilloscope. The temperature was monitored with a thermocouple located as close as possible to the nanophosphor-filled part of the capillary.

The signal amplitude measured in the range 20–150 °C turned out to be an exponential function of temperature. This is characteristic of the thermal quenching of photoluminescence and points to adequate operation of the FOS. At the same time, the optical signal amplitude was found to decrease linearly in the temperature range 150–250 °C and rise sharply above 250 °C. The last result was probably due to the fact that the fibre captured some of the IR radiation resulting from the heating of the wire. Thus, the FOS design in question is unsuitable for high-temperature measurements.

To eliminate the contribution of the IR radiation from the Nichrome wire in detecting the desired signal, the FOS design and measurement procedure were improved. Figure 8 shows a schematic of the updated FOS design, which allows for temperature measurements in the range 20–500 °C.

As seen in Fig. 8, a nanophosphor-containing silica capillary is placed in a stainless steel tube, which shields it from the IR radiation of Nichrome wire heated to above 250 °C. The wire is wound in the form of a few coils onto a ceramic cylinder and potted in a refractory material (fireclay). One advantage of this design is reliable heat insulation, which makes it possible to almost completely avoid heat loss to the ambient atmosphere and localise it as tightly as possible around the capillary. Besides, since the silica capillary was located in the stainless steel tube and there was outer heat insulation, luminescence was excited using a 0.7-m length of large-aperture multimode fibre to deliver excitation light. In the modified FOS design, we used fibre with a core diameter (400 μm) twice that above in order to increase the nanophosphor area to be excited and the photoluminescence signal amplitude. Since the fraction of excitation light that reached the fibre receiving the photoluminescence signal was extremely small, no more than 2% of the total signal, no cut-off filter was used. Besides, since only the nanophosphor-filled end of the capillary underwent maximum heating and only that part of the fibre stripped of its Sn protective coating was exposed to high temperatures, no degradation of the coating occurred above that part.

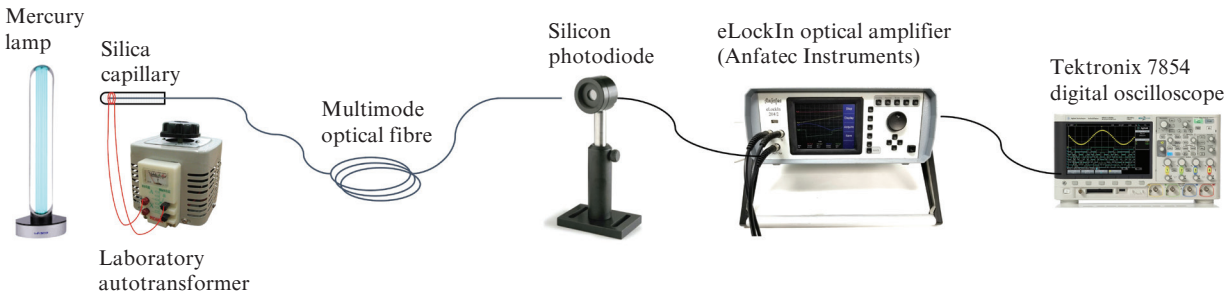

Figure 7. Schematic of the experimental setup used to study the temperature sensitivity of the luminescent FO temperature sensor.

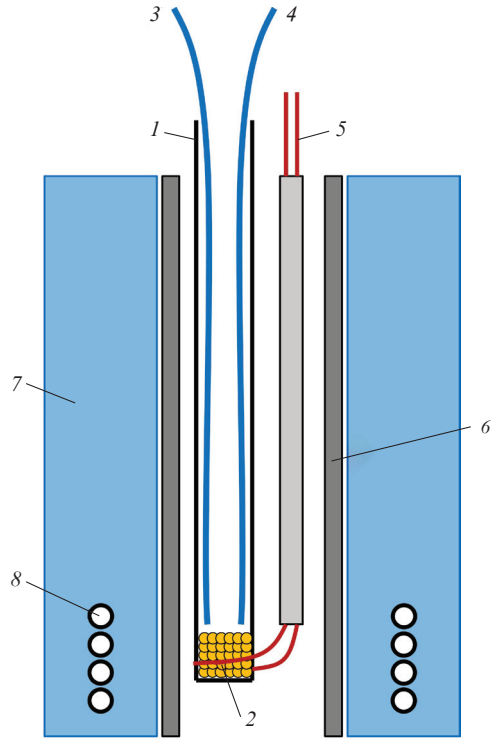

Figure 8. Schematic of the improved luminescent FO temperature sensor design:
(*1*) silica capillary; (*2*) nanophosphor; (*3*) multimode optical fibre for excitation light delivery; (*4*) multimode fibre for photoluminescence signal detection; (*5*) thermocouple; (*6*) stainless steel tube; (*7*) refractory material containing a ceramic cylinder; (*8*) Nichrome wire.

The setup for assessing the temperature sensitivity of the luminescent FO temperature sensor used an OSRAM 64623 HLX halogen lamp, emitting in the range 200–1000 nm, which included all the luminescence excitation wavelengths of the synthesised YAG:R^{3+} (R = Ce, Dy, Yb) nanophosphors. The light from the halogen lamp was focused by a lens onto the entrance slit of an LOMO MDR-23 monochromator, which separated out a 10-nm spectral range for luminescence excitation in the corresponding nanophosphor. The beam from the monochromator output passed through a 50-Hz mechanical chopper and was focused onto a photodetector. In studying the FOS with the YAG:Yb^{3+} nanophosphor, we used a germanium photodiode having the peak sensitivity range 900–1300 nm.

Figure 9 shows the measured photoluminescence signal amplitude as a function of temperature for the synthesised YAG:R^{3+} (R = Ce, Dy, Yb) nanophosphors in FOS's. It is seen that the data are well fitted by a uniformly descending exponential (with a coefficient of determination $R^2 > 0.99$), which points to characteristic thermal quenching of photoluminescence and, accordingly, to adequate operation of the FOS's up to 500 °C. In this case, the main cause of photoluminescence quenching is probably the reduction in the fraction of absorbed light as a consequence of the broadening of the absorption spectrum and the reduction in the absorption coefficient for the excitation light. The data obtained are difficult to interpret in terms of the temperature variation of the luminescence lifetime or decay time because, in the temperature range studied here, these parameters of YAG doped with a moderate concentration of rare-earth ions vary little because of the very low nonradiative relaxation rate [13, 21].

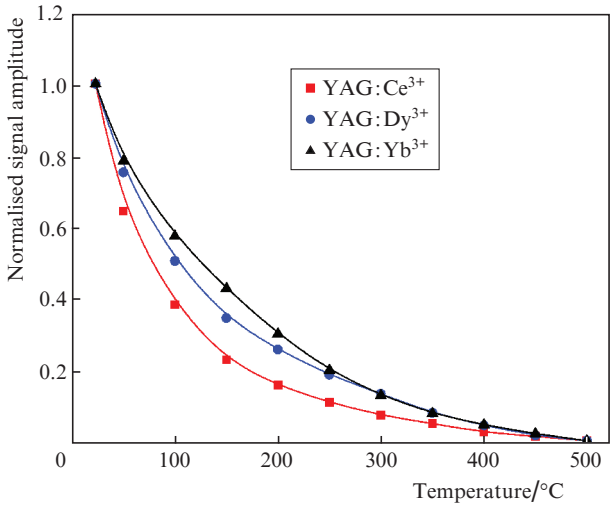

Figure 9. (Colour online) Photoluminescence signal amplitude as a function of temperature for the nanophosphors in FO temperature sensors.

The YAG:Ce^{3+} phosphor ensured the highest FOS sensitivity, i.e. the largest change in photoluminescence signal amplitude over the temperature range of interest, among the nanophosphors synthesised in this study. This can be accounted for by the fact that, unlike Dy^{3+} and Yb^{3+}, Ce^{3+} ions have a *d* electron level, which leads to stronger electronic–vibrational coupling in this element.

4. Conclusions

We have designed a group of luminescent fibre-optic sensors for temperature measurements in the range 20–500 °C, in

which yttrium aluminium garnet nanophosphors doped with 1 wt % trivalent cerium, dysprosium, or ytterbium ions are used as thermosensitive materials. The nanophosphors have been prepared in the form of powders with a crystallite size from 19 to 27 nm by a polymer–salt method and exhibit bright luminescence at 550 (YAG:Ce^{3+}), 400, 480 (YAG:Dy^{3+}), and 1030 nm (YAG:Yb^{3+}). The sensors contain a silica capillary, partially filled with a nanophosphor layer about 3 mm thick, and two large-aperture multimode fibres with a 400-μm-diameter KUVI silica core. The fibres are located in the capillary next to the nanophosphor and are used to deliver excitation light and receive and transmit the photoluminescence signal. The photoluminescence signal amplitude of all the sensors has been shown experimentally to decrease exponentially with increasing temperature, pointing to characteristic thermal quenching of photoluminescence and adequate operation of the devices up to 500 °C. The highest temperature sensitivity is offered by the YAG:Ce^{3+} nanophosphor-based FOS's, which is due to the fact that, unlike Dy^{3+} and Yb^{3+}, Ce^{3+} ions have a *d* electron level, which leads to stronger electronic–vibrational coupling. The proposed sensing element design for FO temperature sensors does not require any precision optical components, which otherwise might be damaged during service under extreme conditions. The sensors can operate in the visible and near-IR spectral regions and are thus reliable and can readily be adapted to existing components and transceiving systems.

Acknowledgements. This work was supported by the Russian Science Foundation (Project No. 19-19-00596).

References

1. Qiao X., Shao Z., Bao W., Rong Q. *Sensors*, **17**, 429 (2017).
2. Liu Y. et al. *Optik*, **132**, 401 (2017).
3. Lin Q., Jiang Z., Zhao N., Yao K., Tian B., Chen F., Shi P. *Sensors*, **18**, 4071 (2018).
4. Yan M., et al. *Sens. Actuators, B*, **255**, 357 (2018).
5. Grattan K.T.V., Sun T. *Sens. Actuators, A*., **82**, 40 (2000).
6. Zhao N. et al. *Sensors*, **18**, 2688 (2018).
7. Jackson R.G. *Novel Sensors and Sensing* (London: CRC Press, 2004).
8. Matrosova A.S., Evstropiev S.K., Mironov L.Yu., Nikonorov N.V., Komarov A.V., Demidov V.V. *Opt. Spectrosc*., **127**, 746 (2019) [*Opt. Spektrosk*., **127**, 692 (2019)].
9. Iida Y., Towata A., Tsugoshi T., Furukawa M. *Vib. Spectrosc.*, **19**, 399 (1999).
10. Denker B., Galagan B., Osiko V., Sverchkov S., Balbashov A.M., Hellström J.E., Pasiskevicius V., Laurell F. *Opt. Commun*., **271**, 142 (2007).
11. Sokolov I.S., Maslennikov S.Y., Evstropiev S.K., Mironov L.Y., Nikonorov N.V., Oreshkina K.V. *Opt. Eng*., **58**, 027103 (2019).
12. Bulyga D.V., Evstropiev S.K., Kuz'menko N.K., Sadovnichii R.V., Nikonorov N.V. *Opt. Spectrosc.*, **129**, 1181 (2021) [*Opt. Spektrosk*., **129**, 1068 (2021)].
13. Hertle E. et al. *J. Lumin*., **182**, 200 (2017).
14. Sevic D. et al. *Eur. Phys. J. D*, **75**, 56 (2021).
15. Evstropiev S.K., Aseev V.A., Demidov V.V., Kuz'menko N.K., Matrosova A.S., Khokhlov A.V., Komarov A.V., Dukelskii K.V., Nikonorov N.V., Oreshkina K.V. *Quantum Electron*., **49**, 1145 (2019) [*Kvantovaya Elektron*., **49**, 1145 (2019)].
16. Matrosova A.S., Kuz'menko N.K., Evstropiev S.K., Aseev V.A., Danilovich D.P., Nikonorov N.V., Ignat'ev A.I., Demidov V.V., Dukelskii K.V. *Opt. Spectrosc*., **129**, in press (2021) [*Opt. Spektrosk*., **129**, 650 (2021)].
17. Rabiei M. et al. *Nanomaterials*, **10**, 1627 (2020).
18. Shannon R.D. *Acta Crystallogr., Sect. A*, **32**, 751 (1976).
19. Bagdasarov Kh.S., Bolotina N.B., Kalinin V.I., Karyagin V.F., Kuz'min B.F., Muradyan L.A., Ryadnov S.N., Uyukin E.M., Chernaya T.S., Fedorov E.A., Chudakov V.S., Simonov V.I. *Sov. Phys. Crystallogr*., **36**, 398 (1991) [*Kristallografiya*, **36**, 715 (1991)].
20. Chemingui S. et al. *J. Lumin*., **166**, 82 (2015).
21. Dramicanin M.D. *Methods Appl. Fluoresc*., **4**, 042001 (2016).